Solving partial differential equations with waveguide-based metatronic networks: supplementary document

Ross Glyn MacDonald,[a,b] Alex Yakovlev,[b] Victor Pacheco-Peña,[a,*]
[a]Newcastle University, School of Mathematics Statistics and Physics, Newcastle Upon Tyne, NE1 7RU, United Kingdom
[b]Newcastle University, School of Engineering, Newcastle Upon Tyne, NE1 7RU, United Kingdom

*Victor Pacheco-Peña, E-mail: victor.pacheco-pena@newcastle.ac.uk

1 Calculating the solution to Poisson equation using a periodic arrangement of resistive elements

It has been described in the main text how a network of lumped elements such as resistors can be used to calculate solutions to the Poisson equation. This is done by emulating the performance of a finite difference grid in a simulation space, shown in[40,41,59]. For completeness, here we provide a brief explanation of this method and derive Eq. 1 from the main text. For further details we refer the readers to[40,41,59]. The structure to solve Poisson equation consists of a periodic arrangement of junctions between lumped elements arranged in a square lattice[40,41,59] (see Fig. S1a). Each junction is connected to four adjacent junctions by a lumped element with an impedance value Z_L, in this way forming a grid-like network. When an external voltage source is applied to one of the boundaries of the network, electric currents will flow through the junctions of the network. These currents will then split at each junction based upon the voltages at the junctions and the impedance values of the lumped elements. If V_0 is the voltage at a center junction and V_a is the voltage value at the adjacent junctions, where $a = 1, 2, 3, 4$ represents the top, right bottom, and left junctions, respectively, the current flowing into the center junction from each of the adjacent junctions is found by using Ohms Law[40,41,59]:

$$I_a = \frac{V_a - V_0}{Z_a} \tag{S1}$$

where, I_a is the current from junction a and Z_a is the impedance value separating junction a from the center junction. The equation governing the voltage distribution of the network can then be found by considering Kirchhoff's laws[64,76] at the junction ($\sum_a I_a = 0$), substituting Eq. S1.

$$\sum_{a=1}^{4} I_a = \frac{V_1}{Z_1} + \frac{V_2}{Z_2} + \frac{V_3}{Z_3} + \frac{V_4}{Z_4} - \left(\frac{1}{Z_1} + \frac{1}{Z_2} + \frac{1}{Z_3} + \frac{1}{Z_4}\right) V_0 = 0 \tag{S2}$$

Eq. 1 from the main text can then be obtained from Eq. S2 for the special case where each of the connected impedance values are the same (i.e., $Z_a = Z_L$). Importantly, any junction which is fully surrounded by adjacent junctions must conform to Eq. S2, as one could relabel any such junction as the center junction 0

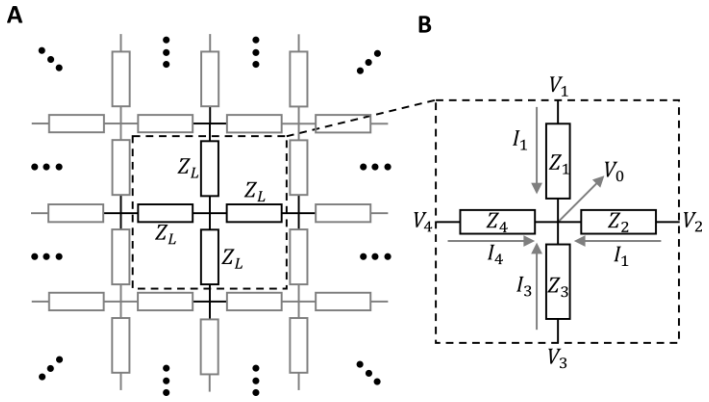

Fig. S1. Grid of interconnected impedances. (a), Schematic representation of the network and (b), unit cell

2 Metatronic circuits in parallel configuration: solution to the Helmholtz equation

As mentioned in the main text, it is also possible to construct a PDE solving structure by instead exploiting waveguide-based metatronic circuits connected in the parallel configuration. To do this, the structure is modified such that the metatronic circuits emulate a Π-circuit instead of the T-circuit discussed in the main text. Additionally, due to the change in configuration, in this scenario the solution to the PDE is now extracted by looking at the out-of-plane E_z-field (and hence voltage value), measured at the center of the junctions.

A schematic representation of this scenario is presented in Fig. S2a where the circuit model of a section of the hypothetical PDE solving structure is shown. It consists of Π-circuits connected at parallel junctions. As in Fig. 1a from the main text, the junctions are arranged in a square lattice with each junction connecting to four adjacent junctions, now via a Π-circuit. The voltages at the adjacent and center junctions are V_a and V_0 respectively, with $a = 1,2,3,4$ representing the top, right, bottom and left connections, respectively. By looking into one of the Π-circuits connected to the center junction, one can calculate an incoming/outgoing current at the center junction (junction 0) as $I_a = (V_a - V_0)/Z_s - V_0/Z_p$, where Z_s and Z_p are now the series and parallel impedance values in the metatronic Π-circuit. The equation governing the voltage distribution of the network is then found by considering Kirchhoffs current law[76] at the center junction $\sum_a^4 I_a = 0$.

$$\frac{V_1 + V_2 + V_3 + V_4 - 4V_0}{Z_s} - \frac{4}{Z_p} V_0 = 0 \tag{S3}$$

By comparing Eq. S3 to the finite difference representation of the Helmholtz equation presented in Eq. 3 of the main text, one can see that the two are analogous if the impedance values are selected so that $Z_s = h^2$ and $Z_p = -4/k^2$. As in the main text, a further

transformation is necessary for this to be strictly valid as $Z_s \in \mathbb{C}$ while $h \in \mathbb{R}$, in this case the required transformation is $V'_a = V_a Z_s^*$ and $V'_0 = V_0 Z_s^*$ which may be substituted into Eq. S3, obtaining:

$$\frac{V'_1 + V'_2 + V'_3 + V'_4 - 4V'_0}{|Z_s|^2} - \frac{4}{Z_p Z_s^*} V'_0 = 0 \tag{S4}$$

which is analogous to Eq. 3 from the main text if the impedances are now selected such that $|Z_s| = h$ and $-4/(Z_p Z_s^*) = k^2$.

The T-circuit required in the PDE solving structure exploited in the main text was implemented using waveguide-based metatronic circuits[49,50,51]. The same principles are also applied here to, instead, implement a metatronic Π-circuit. A schematic representation of the structure is presented in Fig. S2b (top panel). The structure is similar to the one used to emulate the T-circuit from Fig. 1b of the main text, with three thin dielectric/metallic slabs and $\lambda_0/4$ impedance transformers, where λ_0 is the wavelength of the incident signal in free space. However, in this scenario the first and last $\lambda_0/4$ segments have been removed from the structure. The impedance transform[3,50,51] discussed in the main text, is now applied only to the center impedance in order to obtain a central series impedance required for the Π-circuit. The impedance values of the elements in the Π-circuit are calculated using Eq. 6 and Eq. 7 from the main text.

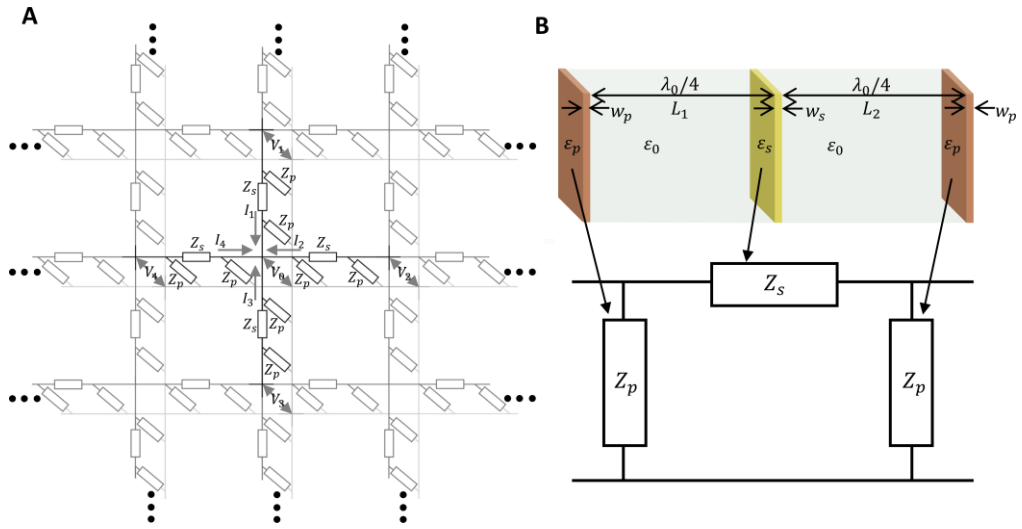

Fig. S2. PDE equation solving structure using Π-circuits and parallel junctions. (a) Schematic representation of the proposed PDE solving structure using Π-circuits and parallel junctions. (b) (Top) Schematic representation of a metatronic circuit using dielectric slabs that would be able to implement the proposed Π-circuit. As in Fig. 1b from the main text this structure consists of 3 dielectric/metallic slabs (one per circuit element) separated by a distance of $\lambda_0/4$, however now the first and last $\lambda_0/4$ blocks have been removed. The width in the direction of propagation and permittivity values of the dielectric slabs are ε_s, ε_p and w_s, w_p, where the subscripts s and p represent the series and parallel elements, respectively. (Bottom) Circuit model of the Π-circuit.

3 ABCD matrix method for extracting and optimizing the equivalent impedance value of the three-slab structure

As discussed in the main text, to corroborate the performance of the designed T-circuit and to extract the emulated impedance values Z_s and Z_p, a full ABCD matrix analysis of the waveguide-based structure is performed. When substituting these impedance values into an ideal T-circuit, the resulting reflection and transmission coefficients should be the same as those using the three-slab structure emulating a T-circuit. However, as discussed in the main text, these values were slightly different from the theoretical impedance values produced via Eq. 6 and Eq. 7 from the main text, due to the non-zero thickness of the dielectric slabs. The method followed to extract and optimize these impedance values is discussed in this section.

To evaluate the performance of the three-slab structure presented in Fig. 1b of the main text, a transmission line (TL) model, shown in Fig. S3, is exploited. It consists of seven TLs representing the three dielectric/metallic slabs, and four air regions between them. The length (along the propagation axis), relative permittivity and characteristic impedances of the TLs representing the dielectric/metallic slabs are $w_{s,p}$, $\varepsilon_{s,p}$ and $Z_{s,p} = Z_0/\sqrt{\varepsilon_{s,p}}$, respectively, where $Z_0 = 120\pi\ \Omega$ is the characteristic impedance of free space and subscripts s, p represent the slabs which enable the emulation of the series and parallel circuit elements, respectively. The air regions within the waveguides between the dielectric slabs are modeled by TLs filled with vacuum (ε_0, Z_0). These TLs have lengths of L_1, L_2, L_3 and L_4, respectively and are all chosen to be $\lambda_0/4$. As it will be discussed later, these values may be carefully modified when optimizing the design to better emulate the performance of an ideal T-circuit with the desired Z_s and Z_p values.

The response of the three-slab structure is calculated by exploiting the ABCD matrix method [9], in which each individual TL is represented by a single ABCD matrix (Υ). The elements for each matrix (A, B, C and D) are as follows:

$$A_{TL} = \cos(\beta d) \tag{S5a}$$

$$B_{TL} = -iZ\sin(\beta d) \tag{S5b}$$

$$C_{TL} = \frac{-i}{Z}\sin(\beta d) \tag{S5c}$$

$$D_{TL} = \cos(\beta d) \tag{S5d}$$

where Z, β and d are the characteristic impedance, propagation constant and length of the TL, respectively. Using Eq. S5, an ABCD matrix is defined for each of the TL segments shown in Fig. S3. These matrices are $\boldsymbol{\Upsilon}_1$, $\boldsymbol{\Upsilon}_2$, $\boldsymbol{\Upsilon}_3$, $\boldsymbol{\Upsilon}_4$, $\boldsymbol{\Upsilon}_{s1}$, $\boldsymbol{\Upsilon}_{s2}$ and $\boldsymbol{\Upsilon}_p$, with 1, 2, 3, 4 as the waveguide regions filled with vacuum ($\lambda_0/4$ waveguides) from left to right (see Fig. S3), s_1, s_2 as the left and right dielectric slabs that enable the emulation of the series impedances and p as the dielectric slab emulating a parallel element. As it is known, the overall ABCD matrix of the structure is then found by multiplying the respective matrices together in order to produce a single ABCD matrix $\boldsymbol{\Upsilon}_T$ which describes the total response of the system.

$$\boldsymbol{\Upsilon}_T = \boldsymbol{\Upsilon}_1\boldsymbol{\Upsilon}_{s1}\boldsymbol{\Upsilon}_2\boldsymbol{\Upsilon}_p\boldsymbol{\Upsilon}_3\boldsymbol{\Upsilon}_{s2}\boldsymbol{\Upsilon}_4 \tag{S6}$$

The values of the emulated series and parallel impedances Z_s, Z_p are found by comparing Eq. S6 with the well-known ABCD matrix of a T-circuit[3]. The ABCD parameters of a T-circuit are as follows:

$$A_{T-circuit} = 1 + \frac{Z_{s1}}{Z_p} \tag{S7a}$$

$$B_{T-circuit} = Z_{s1} + Z_{s2} + \frac{Z_{s1}Z_{s2}}{Z_p} \tag{S7b}$$

$$C_{T-circuit} = \frac{1}{Z_p} \tag{S7c}$$

$$D_{T-circuit} = 1 + \frac{Z_{s2}}{Z_p} \tag{S7d}$$

where Z_p, Z_{s1} and Z_{s2} are the impedances of the parallel, left series and right series components of the T-circuit, respectively. Substituting Eq. 6 and Eq. 7 from the main text into, Eq. S7, the ABCD matrix of the ideal T-circuit ($\boldsymbol{\Upsilon}_{ideal} = \boldsymbol{\Upsilon}_{T-circuit}$). If the matrix components of $\boldsymbol{\Upsilon}_T$ match those from $\boldsymbol{\Upsilon}_{ideal}$, then it can be said that the metatronic elements are emulating the impedances Z_{s1}, Z_{s2} and Z_p correctly. However, it was found that there was indeed a slight variation between these two matrices, and thus also a slight variation in the emulated impedance values. The true impedance values emulated by the three-slab structure can then be calculated by substituting the ABCD matrix parameters from $\boldsymbol{\Upsilon}_T$ into Eq. S7, to construct a series of simultaneous equations, which can then be solved for Z_{s1}, Z_{s2} and Z_p. The result of this calculation was then presented in the section "Emulating T-circuit lumped elements via metatronic circuit elements" from the main text.

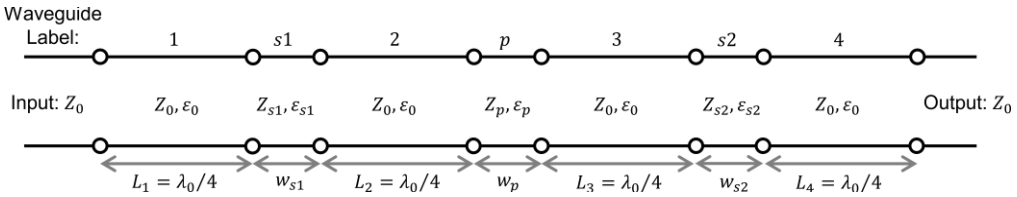

Fig. S3. Three-slab transmission line model. Full TL model of the three-slab structure designed to emulate a T-circuit. TLs 1, 2, 3 and 4 are the four $\lambda_0/4$ sections while $s1$, $s2$ and p are the dielectric/metallic slabs which enable the emulation of the left series, right series, and parallel impedances respectively. Each TL is parameterized by the characteristic impedance, permittivity, and length of the TL. TLs 1,2,3 and 4 have the impedance permittivity and length values Z_0, ε_0 and $L_{1,2,3,4}$, respectively. The TLs representing the dielectric slabs $s1$, $s2$ and p have the impedance, permittivity, and length values $Z_{s1,s2,p}$, $\varepsilon_{s1,s2,p}$ and $w_{s1,s2,p}$, respectively. Connecting to the left and right of the structure are the input and output TLs respectively with a characteristic impedance Z_0.

For completeness, the ABCD parameters, reflection/transmission coefficients and impedance values for the structure discussed in Fig. 1 of the main text are presented in column 2 of Table. S1. Here, the desired impedance values of the metatronic elements are $Z_{s1} = Z_{s2} = -0.9iZ_0$ and $Z_p = 2.5iZ_0$, respectively. Metatronic elements capable of emulating these impedance values are then designed using Eq. 6 and Eq. 7 from the main text, with the geometric parameters and EM properties as follows: $w_{s1} = w_{s2} = w_p = 0.2$ mm ($\lambda_0/150$ where $\lambda_0 = 30$ mm), $\varepsilon_{s1} = \varepsilon_{s2} = 21.44$, $\varepsilon_p = 9.54$ and $L_1 = L_2 = L_3 = L_4 = 7.5$ mm ($\lambda_0/4$). Using these geometric parameters ($L_{1,2,3,4}$, $w_{s1,s2,p}$) and EM properties ($\varepsilon_{s1,s2,p}$), the ABCD matrix components, reflection/transmission coefficient and emulated impedance values of the three-slab structure are calculated using Eq. S5-S7. These results are shown in the third column of Table. S1. As it can be seen, there is a slight difference between the desired impedance values and the emulated impedance values. In order to better implement the desired impedance values, an optimization of the geometrical parameters (L_1, L_2, L_3, L_4, w_{s1}, w_{s2}, w_p) and EM properties (ε_{s1}, ε_{s2}, ε_p) of the structure is performed to minimize the objective function:

$$O\left(Z_{s1}, Z'_{s1}, Z_{s2}, Z'_{s2}, Z_p, Z'_p\right) = |Z_{s1} - Z'_{s1}| + |Z_{s2} - Z'_{s2}| + |Z_p - Z'_p| \qquad \text{(S8)}$$

where Z_{s1}, Z_{s2}, Z_p are now the emulated impedances of the left series, right series and parallel elements calculated for the three-slab structure using Eq. S5-S7 and Z'_{s1}, Z'_{s2}, Z'_p are the desired impedance values of the left series, right series and parallel elements (i.e. in this example $Z'_{s1} = Z'_{s2} = -0.9iZ_0$ and $Z_p = 2.5iZ_0$). The results, after the optimization to minimize Eq. S8, are presented in column 4 of Table. S1. The optimized parameters are: $\varepsilon_{s1} = \varepsilon_{s2} = 21.5$, $\varepsilon_p = 12$, $w_{s1} = w_{s2} = 0.2111$ mm, $w_p = 0.1741$ mm, $L_1 = L_4 = 7.3944$ mm and $L_2 = L_3 = 7.3074$ mm. With these new parameters, the impedance values (which are emulated by the three-slab structure) are now in agreement with the desired impedance values to three significant figures. This optimized structure is used to produce the results shown in Fig. 2d from the main text.

Parameter	T-circuit	Three-slab structure with initial parameters	Optimized three-slab structure
A	0.6409	0.5674	0.6396
B	$-1.474iZ_0$	$-1.459iZ_0$	$-1.476iZ_0$
C	$\frac{-0.3998i}{Z_0}$	$\frac{-0.4646i}{Z_0}$	$\frac{-0.4003i}{Z_0}$
D	0.6409	0.5674	0.6396
Γ	$0.3906 - 0.2671i$	$0.3836 - 0.2262i$	$0.3914 - 0.2668i$
T	$0.4974 + 0.7271i$	$0.4548 + 0.7712i$	$0.4961 + 0.7277i$
Z_{s1}	$-0.9iZ_0$	$-0.9311iZ_0$	$-0.9002iZ_0$
Z_{s2}	$-0.9iZ_0$	$-0.9311iZ_0$	$-0.9002iZ_0$
Z_p	$2.5iZ_0$	$2.152iZ_0$	$2.498iZ_0$

Table S1. EM response of the ideal T-circuit, three-slab structure and optimized three slab structure. The ABCD parameters, reflection and transmission coefficients are presented for the ideal T-circuit, the initial three-slab structure and the optimized three-slab structure are presented in columns 2, 3 and 4 respectively. The impedance values used to calculate the ideal T-circuit response and the calculated impedance values of the initial and optimized three-slab structure are presented in the bottom three rows of columns 2, 3 and 4 respectively.

4 Method for calculating the theoretical H_z-field at the junctions of metatronic circuits

Consider an arbitrary sized network of series junctions between T-circuits, as is presented in Fig. 2 of the main text. Such a network can be decomposed into two sets of components: 1) the junctions and 2) the T-circuits connecting the junctions together. Both components can be characterized by a scattering matrix A, with A_J and A_T as the scattering matrix of the junctions and T-circuits respectively. The scattering matrix relates the vector of incident signals $x = [x_1, x_2, \ldots x_N]^T$ to the vector of output signals $y = [y_1, y_2, \ldots y_N]^T$, where the superscript T indicates the transpose operation and N is the number of inputs/outputs of the scattering matrix (i.e. $N = 2$ and $N = 4$ for the T-circuits and junctions respectively). As mentioned in the main text, in this work the filling materials and dimensions of all waveguides is the same (i.e. the characteristic impedance of all waveguides is the same). When this is the case, as it has been shown in previous works[64,65,66,70], the scattering matrix of a series junction (considering ideal interconnected TLs) is given by $A_J = I - \gamma J$, where I, J are the 4×4 identity and all-ones matrices, respectively and $\gamma = 1/2$ is the transmission coefficient of the structure. The scattering matrix of the T-circuit is found from its ABCD parameters after substituting the emulated impedance values, using the method described in section S3. It is important to note that if the PDE to be solved is inhomogeneous, such as the case presented in Fig. 4d from the main text, the scattering matrix will vary between T-circuits. Due to this it is important to define to which junctions the T-circuits are connected.

Once the scattering matrices have been constructed and the connections between them have been defined, the behavior of the total network is solved by systematically combining the scattering matrices of connected structures (junctions and T-circuits), until all the junctions and T-circuits are included into one final scattering matrix that describes the whole system. To better visualize this, the signal flow graph[3] for a small section of the network (a four-way

junction and a single connected T-circuit, to the right, as seen in the insert of Fig. S4a) is presented in Fig. S4a. The inputs and outputs seen at the waveguide junction are represented by the nodes labeled x_a and y_a, respectively, where $a = 1, 2, 3, 4$ is representative of the direction from which the signals arrive or are depart towards (up, right, down, and left, respectively). The arrows between nodes represent the connections between inputs and outputs. The remaining arrows represent the external connections between the displayed structure and the rest of the network. The scattering of signals between the inputs and outputs of the four-way junction form the octagon shaped section of the signal flow diagram. The nodes within the black dashed box represent the T-circuit connected to the right of the scattering matrix and the terms x'_2 and y'_2 represent the input/output signals at the righthand side of the T-circuit. An observation node is also included (grey circle), which is a purely mathematical tool used to observe the signals propagating away from the junction so that the current around the junction I_0 may be recorded. The overall scattering matrix of the junction and T-circuit structure can then be found by systematically implementing the signal flow graph decomposition rules[3] to eliminate unnecessary nodes from the diagram and, in doing so, constructing a new scattering matrix for the combined structure $\boldsymbol{A'}$ with inputs and outputs vectors as $\boldsymbol{x'}$ and $\boldsymbol{y'}$, respectively. An example of this is presented in Fig. S4b where the calculation the A'_{22} term of the combined scattering matrix is shown. The leftmost panel shows a reduced signal flow diagram for the T-circuit (inside the dashed box in Fig. S4a) and input/output 2 of the scattering matrix. For clarity, connections not involved in the calculation of A'_{22} are replaced with grey arrows. Between the left panel and the middle panel from the same Fig. S4b, the loop created between the S_{11} term of the T-circuit and the A_{22} term of the junction, is reduced to a single connection. This is to enable the representation of the total reflection between the T-circuit and junction.

As observed, this new connection is also part of another loop consisting of itself, and the S_{21}, S_{12} terms of the T-circuit. This means that this final loop can be reduced into the final connection A'_{22} shown on the right panel from Fig. S4b, which describes the total reflection by the combined T-circuit and junction structure.

A visual representation of this algorithm is presented in Fig. S5. In this example the algorithm is applied to a 2×2 network of junctions, shown in Fig. S5a. In this schematic, the scattering matrix of the junctions $\boldsymbol{A}_J$ and T-circuits $\boldsymbol{A}_T$ are represented by the black and blue boxes, respectively. To demonstrate the generality of this method, each T-circuit is assigned an individual scattering matrix $\boldsymbol{A}_{T_a}$ with $a = 1, 2, 3, 4$ representing the top, right, bottom and left T-circuits, respectively. Connections between the scattering matrices are depicted by grey arrows. As the algorithm is applied, connected scattering matrices are combined into and replaced by the scattering matrix $\boldsymbol{A}'$. This can be seen in Fig. S5b, which shows the structure after one combination between the scattering matrices of the top-left junction ($\boldsymbol{A}_J$) and the top T-circuit ($\boldsymbol{A}_{T_1}$), seen in Fig. S5a. Importantly, $\boldsymbol{A}'$ inherits the connections from both the scattering matrices used to construct it. This can also be seen in Fig. S5b where $\boldsymbol{A}'$ is connected to both the left T-circuit (inherited from the top left junction) and the top-right junction (inherited from the top T-circuit). This process is repeated, with each step adding a new scattering matrix to the overall structure and, in doing so, a new $\boldsymbol{A}'$ is constructed at each stage. For example, in the next step, the scattering matrix $\boldsymbol{A}'$, is combined with the scattering matrix of the top-right junction $\boldsymbol{A}_J$, and a new $\boldsymbol{A}'$, is constructed that includes the three scattering matrices from the top row of Fig. S5a. The structure after 6 iterations is presented in Fig. S5c. Here, all scattering matrices, except the bottom-right junction, have been added into the combined scattering matrix $\boldsymbol{A}'$. This iteration is significant as it highlights the scenario where

there is more than one connection between the combined scattering matrix $\boldsymbol{A}'$ and the scattering matrix to be added at the next step (the scattering matrix of the bottom right junction).

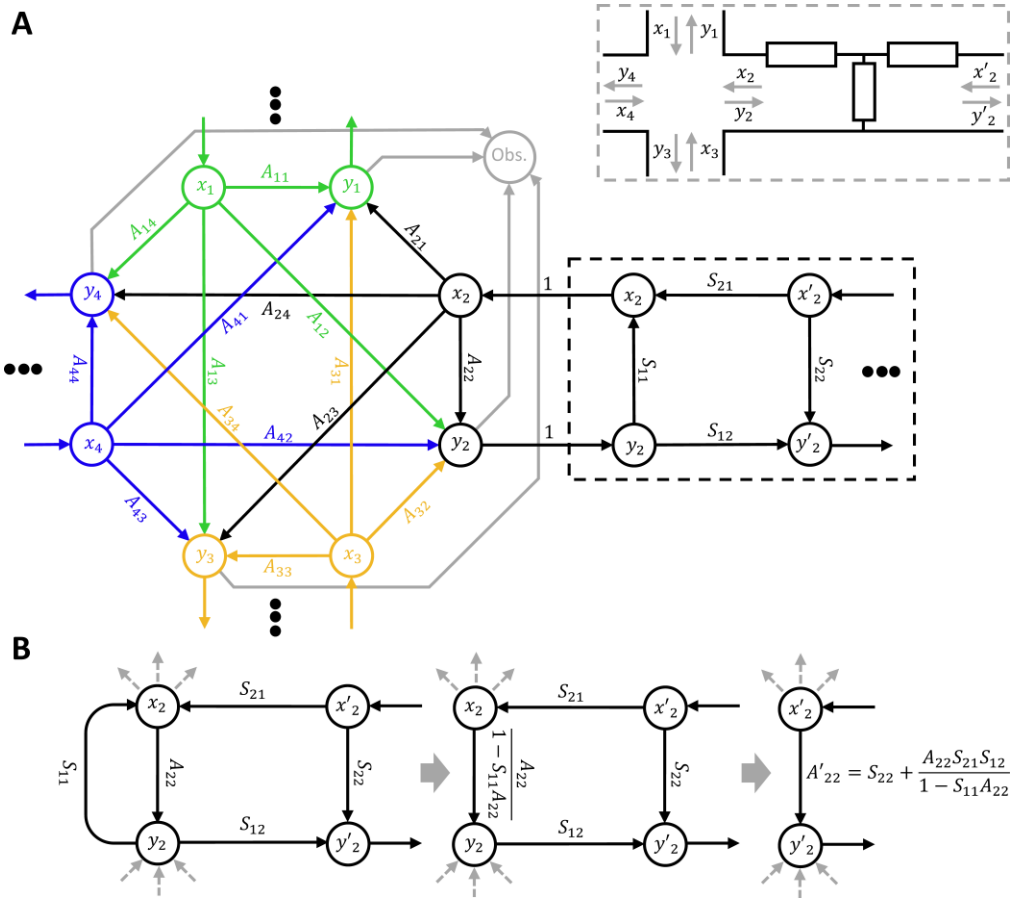

Fig. S4. Waveguide junction signal flow diagram. (a), Signal flow diagram showing the splitting and superposition of signals at a series junction and a connected T-circuit (see insert). The nodes within the dashed box are representative of the T-circuit while the remaining nodes represent the four-waveguide junction. The incident and outgoing signals at the junction are labeled as x and y, respectively, with the numbered subscript indicating from which adjacent junction the signals arrive from (1 up, 2 right, 3 down and 4 left). x'_2 and y'_2 indicate the signals from the righthand junction which are separated from the main junction by the T-circuit. Signal flow routes around the junction are color coordinated to indicate which adjacent junction they connect to (green up, black right, orange down and blue left). (b), Schematic example of the signal flow diagram associated with the T-circuit may be combined with the 4-way junction to construct a combined signal flow diagram.

A general example of this scenario is also presented in Fig. S5d. Here, two systems described by the scattering matrices $\boldsymbol{A}'$ and $\boldsymbol{A}$ share M connections. These systems also have N' and N external input/output waveguides, respectively. This means that, in this scenario, $\boldsymbol{A}'$ and $\boldsymbol{A}$ will consist of $(N'+M)\times(N'+M)$ and $(N+M)\times(N+M)$ terms, respectively. Likewise, the

input and output vectors $\boldsymbol{x}$, $\boldsymbol{x}'$ and $\boldsymbol{y}$, $\boldsymbol{y}'$ consist of $N' + M$ and $N + M$ terms for the dashed and undashed vectors respectively. When constructing $\boldsymbol{x}$, $\boldsymbol{x}'$ $\boldsymbol{y}$ and $\boldsymbol{y}'$, the terms of the vectors are arranged such that the elements x_a, ${x'}_a$, y_a and y'_a for $a = 1,2,\ldots,M$ are input/output signals from/towards a connection between the two systems. Additionally, care is taken so that for each a, x_a, ${x'}_a$, y_a and y'_a are signals from/towards the same connection for both the dashed and undashed terms. The remaining N' and N term of $\boldsymbol{x}'$, $\boldsymbol{y}'$ and $\boldsymbol{x}$, $\boldsymbol{y}$ respectively, are then the external inputs/outputs of each system. With this labeling convention, the terms of the output vectors $\boldsymbol{y}$ and $\boldsymbol{y}'$ may be rewritten as

$$y'_{j'} = \sum_{a_1=1}^{M} \boldsymbol{A}'_{j',a_1} {x'}_{a_1} + \sum_{a_2=M+1}^{M+N'} \boldsymbol{A}'_{j',a_2} {x'}_{a_2} \tag{S9a}$$

$$y_j = \sum_{b_1=1}^{M} \boldsymbol{A}_{j,b_1} x_{b_1} + \sum_{b_2=M+1}^{M+N} \boldsymbol{A}_{j,b_2} x_{b_2} \tag{S9b}$$

where $j' = 1, 2, \ldots N' + M$ and $j = 1, 2, \ldots N + M$ is the output number of the outgoing signals from the dashed and undashed system, respectively. In Eq. S9a,b, the first and second terms describe the scattering towards an output due to signals originating from a connection and from an external input, respectively. Due to the connections between scattering matrices and the vector ordering described above, the first M outputs of the dashed system then become the first M inputs of undashed system and vice versa. This may be expressed as

$${x'}_m = y_m \tag{S10a}$$

$$x_m = {y'}_m \tag{S10b}$$

when $m = 1, 2, \ldots M$. Considering Eq. S10, Eq. S9 can be rewritten as follows.

$$y'_{j'} = \sum_{a_1=1}^{M} \boldsymbol{A'}_{j',a_1} y_{a_1} + \sum_{a_2=M+1}^{M+N'} \boldsymbol{A'}_{j',a_2} x'_{a_2} \tag{S11a}$$

$$y_j = \sum_{b_1=1}^{M} \boldsymbol{A}_{j,b_1} y'_{b_1} + \sum_{b_2=M+1}^{M+N} \boldsymbol{A}_{j,b_2} x_{b_2} \tag{S11b}$$

Importantly, as the two systems are linked, Eq. S11a appears in the first term of Eq. S11b when $j' = b_1 = 1$ to M. Likewise, Eq. S11b appears in the first term of Eq. S11a for $j = a_1 = 1$ to M. Eq. S11a and Eq. S11b are then combined to give:

$$y'_{j'} = \sum_{a_1=1}^{M} \sum_{b_1=1}^{M} \boldsymbol{A'}_{j',a_1} \boldsymbol{A}_{a_1,b_1} y'_{b_1} + \sum_{a_1=1}^{M} \sum_{b_2=M+1}^{M+N} \boldsymbol{A'}_{j',a_1} \boldsymbol{A}_{a_1,b_1} x_{b_2} + \sum_{a_2=M+1}^{M+N'} \boldsymbol{A'}_{j',a_2} x'_{a_2} \tag{S12a}$$

$$y_j = \sum_{b_1=1}^{M} \sum_{a_1=1}^{M} \boldsymbol{A}_{j,b_1} \boldsymbol{A'}_{b_1,a_1} y_{a_1} + \sum_{b_1=1}^{M} \sum_{a_2=M+1}^{M+N'} \boldsymbol{A}_{j,b_1} \boldsymbol{A'}_{b_1,a_2} x'_{a_2} + \sum_{b_2=M+1}^{M+N} \boldsymbol{A}_{j,b_2} x_{b_2} \tag{S12b}$$

which are a pair of simultaneous equations that may be solved to obtain y' and y in terms of the input signals and scattering matrix coefficients only. To do this we define two $M \times M$ matrices $\boldsymbol{B'}$ and $\boldsymbol{B}$ as:

$$\boldsymbol{B'}_{m',m} = \sum_{c=1}^{M} \boldsymbol{A'}_{m',c} \boldsymbol{A}_{c,m} \tag{S13a}$$

$$\boldsymbol{B}_{m,m'} = \sum_{c=1}^{M} \boldsymbol{A}_{m,c} \boldsymbol{A'}_{c,m'} \tag{S13b}$$

where $m' = 1, 2, \ldots M$. By Substituting the terms of $\boldsymbol{B'}$ and $\boldsymbol{B}$ into Eq. 12a and Eq. 12b, respectively, the output signals in the connecting waveguides (waveguides 1 to M) are expressed as:

$$y'_{j'} = \sum_{c=1}^{M}\sum_{a_1=1}^{M}\sum_{b_2=M+1}^{M+N}(\boldsymbol{I}-\boldsymbol{B}')^{-1}_{j',c}\boldsymbol{A}'_{c,a_1}\boldsymbol{A}_{a_1,b_2}x_{b_2} + \sum_{c=1}^{M}\sum_{a_2=M+1}^{M+N'}(\boldsymbol{I}-\boldsymbol{B}')^{-1}_{j',c}\boldsymbol{A}'_{c,a_2}x'_{a_2} \quad \text{(S14a)}$$

$$y_j = \sum_{c=1}^{M}\sum_{b_1=1}^{M}\sum_{a_2=M+1}^{M+N'}(\boldsymbol{I}-\boldsymbol{B})^{-1}_{j,c}\boldsymbol{A}_{c,b}\boldsymbol{A}'_{b,a_2}x'_{a_2} + \sum_{c=1}^{M}\sum_{b_2=M+1}^{M+N}(\boldsymbol{I}-\boldsymbol{B})^{-1}_{j,c}\boldsymbol{A}_{c,b_2}x_{b_2} \quad \text{(S14b)}$$

where $\boldsymbol{I}$ is the identity matrix with size $M \times M$. Substituting the expressions from Eq. S14a and Eq. S14b into Eq. S11b and Eq. S11a, respectively, gives the equations for the external outputs of either system as:

$$y'_{(M+\nu')} = \sum_{a_2=M+1}^{M+N'}[\boldsymbol{A}'_{(M+\nu'),a_2} + \sum_{a_1=1}^{M}\sum_{c=1}^{M}\sum_{b_1=1}^{M}\boldsymbol{A}'_{(M+\nu'),a_1}(\boldsymbol{I}-\boldsymbol{B})^{-1}_{a_1,c}\boldsymbol{A}_{c,b_1}\boldsymbol{A}'_{b_1,a_2}]\,x'_{a_2} + \sum_{a_1=1}^{M}\sum_{c=1}^{M}\sum_{b_2=M+1}^{M+N}\boldsymbol{A}'_{(M+\nu'),a_1}(\boldsymbol{I}-\boldsymbol{B})^{-1}_{a_1,c}\boldsymbol{A}_{c,b_2}x_{b_2} \quad \text{(S15a)}$$

$$y_{(M+\nu)} = \sum_{b_2=M+1}^{M+N}[\boldsymbol{A}_{(M+\nu),b_2} + \sum_{b_1=1}^{M}\sum_{c=1}^{M}\sum_{a_1=1}^{M}\boldsymbol{A}_{(M+\nu),b_1}(\boldsymbol{I}-\boldsymbol{B}')^{-1}_{b_1,c}\boldsymbol{A}'_{c,a_1}\boldsymbol{A}_{a_1,b_2}]x_{b_2} + \sum_{b_1=1}^{M}\sum_{c=1}^{M}\sum_{a_2=M+1}^{M+N'}\boldsymbol{A}_{(M+\nu),b_1}(\boldsymbol{I}-\boldsymbol{B}')^{-1}_{b_1,c}\boldsymbol{A}'_{c,a_2}x'_{a_2} \quad \text{(S15b)}$$

where $\nu' = 1, 2, \ldots N'$ and $\nu = 1, 2, \ldots N$ are the external input/output numbers of the dashed and undashed systems, respectively. The matrix elements for the combined scattering matrix of the structure are then extracted from Eq. S15. In this instance, the combined scattering matrix (between Eq. S15a and Eq. S15b) is written as $\boldsymbol{A''}$ to avoid confusion with the input matrix $\boldsymbol{A'}$. However, as detailed above, when combining multiple scattering matrices sequentially to calculate the scattering matrix of the entire network, $\boldsymbol{A''}$ would take the place of $\boldsymbol{A'}$ in subsequent calculations. This process is shown in Fig. S5a-c. The input and output vectors of $\boldsymbol{A''}$ are $\boldsymbol{x''} = [x''_1, x''_2, \ldots x''_{N+N'}]^T$ and $\boldsymbol{y''} = [y''_1, y''_2, \ldots, y''_{N+N'}]^T$. These are vectors contains the combined external input/output terms from $\boldsymbol{x}$, $\boldsymbol{x'}$ and $\boldsymbol{y}$, $\boldsymbol{y'}$, respectively. In this formulation the first N' terms of $\boldsymbol{x''}$ and $\boldsymbol{y''}$ are the terms of $\boldsymbol{x'}$ and $\boldsymbol{y'}$ (ordered $1, 2, \ldots N'$) and the remaining N terms represent the terms of $\boldsymbol{x}$ and $\boldsymbol{y}$ (ordered $1, 2, \ldots N$), respectively (i.e. $x''_{\nu'} = x'_{(\nu'+M)}$, $y''_{\nu'} = y'_{(\nu'+M)}$, $x''_{(\nu+N')} = x_{(\nu+M)}$ and $x''_{(\nu+N')} = x_{(\nu+M)}$). The individual terms of $\boldsymbol{A''}$ are then written as:

$$\boldsymbol{A''}_{\nu',\nu'_2} = \boldsymbol{A'}_{(M+n'),(M+n'_2} + \sum_{a_1=1}^{M}\sum_{c=1}^{M}\sum_{b_1=1}^{M} \boldsymbol{A'}_{(M+\nu'),a_1}(\boldsymbol{I}-\boldsymbol{B})^{-1}_{a_1,c}\boldsymbol{A}_{c,b_1}\boldsymbol{A'}_{b_1,(M+\nu'_2)} \tag{S16a}$$

$$\boldsymbol{A''}_{\nu',(\nu+N')} = \sum_{a_1=1}^{M}\sum_{c=1}^{M} \boldsymbol{A'}_{(M+\nu'),a_1}(\boldsymbol{I}-\boldsymbol{B})^{-1}_{a_1,c}\boldsymbol{A}_{c,(M+\nu)} \tag{S16b}$$

$$\boldsymbol{A''}_{(n+N'),n'} = \sum_{b_1=1}^{M}\sum_{c=1}^{M} \boldsymbol{A}_{(M+n),b_1}(\boldsymbol{I}-\boldsymbol{B'})^{-1}_{b_1,c}\boldsymbol{A'}_{c,(\nu'+M)} \tag{S16c}$$

$$\boldsymbol{A''}_{(\nu+N'),(\nu_2+N')} = \boldsymbol{A}_{(M+\nu),(M+\nu_2)} + \sum_{b_1=1}^{M}\sum_{c=1}^{M}\sum_{a_1=1}^{M} \boldsymbol{A}_{(M+\nu),b_1}(\boldsymbol{I}-\boldsymbol{B'})^{-1}_{b_1,c}\boldsymbol{A'}_{c,a_1}\boldsymbol{A}_{a_1,(\nu_2+M)} \tag{S16d}$$

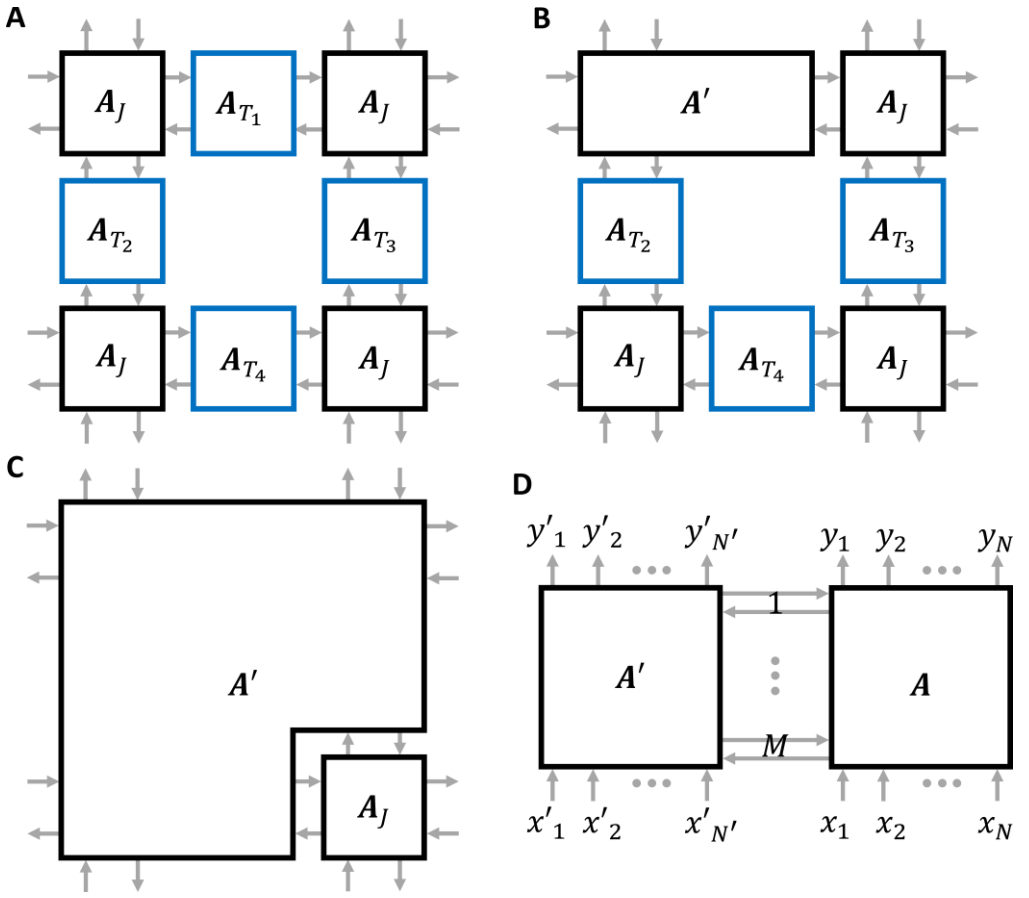

Fig. S5. Schematic representation of the algorithm used to solve for the theoretical results of current/H-field distribution. (a) Initial state of a 2×2 network to be solved by the scattering matrix combining algorithm. The waveguide junctions and T-circuits are modelled as 4×4 and 2×2 scattering matrices $\boldsymbol{A}_J$ and $\boldsymbol{A}_{T_a}$, respectively, represented by black and blue boxes. $a = 1, 2, 3, 4$ is the T-circuit number, in this case referring to the top, right, bottom, and left T-circuits of the structure, respectively. (b) State of the network after one scattering matrix combination. The scattering matrix of the top-left junction has been combined with the scattering matrix of the top T-circuit. In doing so, the combined scattering matrix of the two structures is constructed. $\boldsymbol{A}'$, inheriting the connections from both scattering matrices. (c) State of the network, after the penultimate iteration. Here, all but the scattering matrix of the bottom-right junction have been combined into the overall scattering matrix $\boldsymbol{A}'$. In this scenario, $\boldsymbol{A}'$ is connected to the scattering matrix to be added $\boldsymbol{A}$, by 2 connections, one left of and one above $\boldsymbol{A}$. (d) General case of two scattering matrices connected by an arbitrary number of connections. Here the scattering matrices $\boldsymbol{A}'$ and $\boldsymbol{A}$ are connected by M reciprocal connections, represented by the grey arrows between the two black boxes. $\boldsymbol{A}'$ and $\boldsymbol{A}$ have N' and N input/outputs respectively, which do not connect the two scattering matrices, represented by the grey arrows above and below the box.

5 Impact of manufacturing tolerance on the calculated PDE solution

5.1 Changing Z_s and Z_p from ideal values:

The structures discussed in the main text have considered defined values of Z_s and Z_p. In practice, these values may diverge from the ideal values due to potential manufacturing tolerances. To investigate the impact of these tolerances and the error associated to the PDE solution, it is important to consider how perturbations in Z_s and Z_p around their ideal values impact the observed values of h and k i.e. $Z_s \to Z_s + \Delta Z_s$, $Z_p \to Z_p + \Delta Z_p$, $h \to h + \Delta h$ and $k \to k + \Delta k$, where ΔZ_s, ΔZ_p, Δh and Δk are the amounts by which Z_s, Z_p, h and k are perturbed, respectively. Using $h = 1/|Z_p|$ and $k = \sqrt{-4Z_s Z_p^*}$ from the main text, the values of Δh and Δk can be defined as, respectively.

$$\Delta h \approx -\frac{\Delta Z_p}{Z_p^2} \tag{S17a}$$

$$\Delta k \approx \frac{1}{\sqrt{-Z_s Z_p^*}}(Z_s \Delta Z_p + Z_p^* \Delta Z_s) \tag{S17b}$$

The results from these expressions are shown in Fig. S6 in which the values of Δh and Δk have been calculated for ΔZ_s and ΔZ_p between -5% and $+5\%$ of Z_s and Z_p, respectively. In this scenario $Z_s = -0.9i$ and $Z_p = 2.5i$ corresponding to $h = 0.4$ and $k = 3$. Additionally, Fig. S6c shows the RMSE between the perturbed and unperturbed theoretical PDE solutions. As it can be seen, there are non-zero combinations of ΔZ_s and ΔZ_p which produce solutions similar to $\Delta Z_s = 0$ and $\Delta Z_p = 0$, despite using different values of h and k. This occurs when the value of $1/(hk)$ is kept constant between the set of solutions.

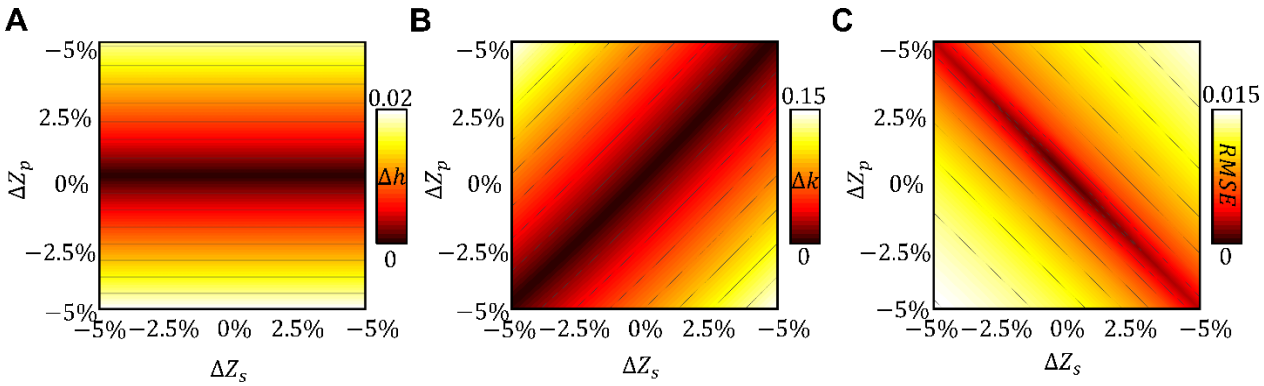

Fig. S6. Impact of perturbations in Z_s and Z_p. (a-b) calculated Δh and Δk value for ΔZ_s and ΔZ_p values within 5% of Z_s and Z_p, respectively. These results are calculated when $Z_s = -0.9i$ and $Z_p = 2.5i$. (c) Calculated RMSE between the theoretical PDE solutions of the perturbed and unperturbed structures.

Now using Eq. S17 the distribution of h and k values seen in a system with impedance tolerances can be calculated. To do this we initially consider an equal probability distribution of impedances between $Z_{s,p} - \delta Z_{s,p}$ and $Z_{s,p} + \delta Z_{s,p}$ where $\delta Z_{s,p}$ is the tolerance of Z_s and Z_p, respectively. The joint probability distribution of h and k due to the presence of δZ_s and δZ_p is then calculated. This can be seen in Fig. S7a when δZ_s and δZ_p are chosen to be 5% of Z_s and Z_p, respectively. Here, h and k values are calculated for 1000 equally spaced values of Z_s and Z_p within the tolerance range. The number of combinations which produce similar h and k values are then counted. As it can be seen, since Δh is a linear function of ΔZ_p only, the equal distribution of Z_p values also translate to an equal distribution in h values. This means that a 5% tolerance in Z_p will produce h values within 5% of the desired value. Since Δk depends on both ΔZ_s and ΔZ_p, the joint distribution of the two impedances produces a spread of k values centered around the desired value ($k = 3$ in this case). The standard deviation (STD) of the k value is then calculated for a range of tolerance values and is show in Fig. S7b. From these results, for instance, if the impedance tolerance was 5% one would expect to measure h and k values within the ranges $h = [0.38, 0.42]$ and $k = [2.63, 3.37]$, respectively.

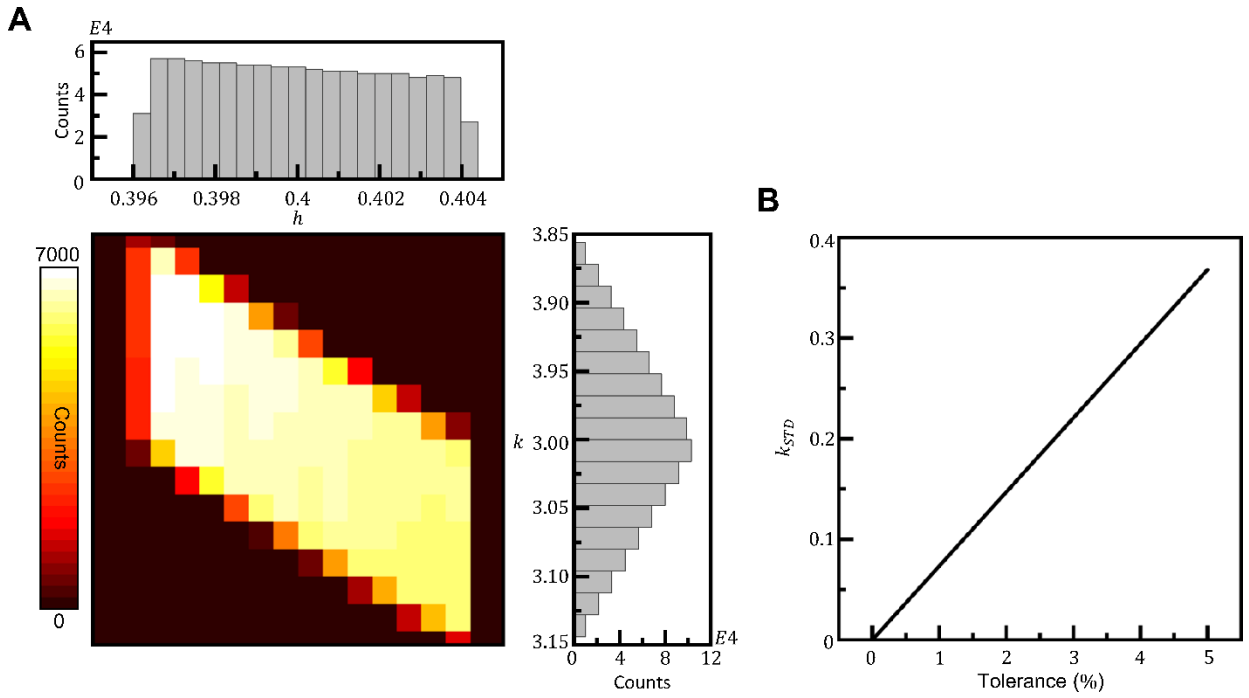

Fig. S7. Distribution of h and k values with impedance tolerances. (a) 2D histogram showing the distribution of h and k values around $h = 4$ and $k = 3$ when Z_s and Z_p is allowed to vary by 5% around $Z_s = -0.9i$ and $Z_p = 2.5i$. (b) Calculated standard deviation of k value from the k distribution for tolerance levels from 0% to 5%.

5.2 Geometry tolerances:

As shown in the main text, Z_s and Z_p may be emulated by controlling the geometric parameters and electromagnetic properties of the three-slab structure shown in Fig. 1b. These parameters are L_1, L_2, L_3,L_4, w_{s1}, w_{s2},w_p, ε_{s1}, ε_{s2} and ε_p. One alternative method for evaluating the error and the h and k distribution is to consider the impact of tolerances on these underlying parameters/properties. This is different than the study presented above as in this scenario it is expected that there will no longer be an equal distribution of Z_s and Z_p values. Similar to the study above, L_1, L_2, L_3,L_4, w_{s1}, w_{s2},w_p, ε_{s1}, ε_{s2} and ε_p are now allowed to vary by δL_1, δL_2, δL_3,δL_4, δw_{s1}, δw_{s2},δw_p, $\delta \varepsilon_{s1}$, $\delta \varepsilon_{s2}$ and $\delta \varepsilon_p$, respectively, around the desired values. For this study, the parameters and properties described in Fig. 2d from the main text are chosen as the desired values (i.e. $h = 0.4003$, $k = 2.999$). Due to the large parameter space (10 variables in total) the h and k distribution is then evaluated by selecting 100000 randomly chosen

combinations of parameters within the parameter space and counting the combinations which produce similar values of h and k. The results of which can be seen in Fig. S8a when δL_1, δL_2 … $\delta\varepsilon_p$ are 5% of the desired value. The mean value and standard deviation of these distributions is then evaluated by using a gaussian and skewed gaussian fit[77] for the for the h and k distributions respectively. Fig. S8b shows the normalized fits for tolerance values from 1% to 5%. These fits are normalized such that the integral of each curve (representing the total number of sampling points) is the same in each plot. Finally, the extracted mean and standard deviation values of h and k are show in Fig. S8c. These results show that for a tolerance value of 5% on the underlying T-circuit parameters/properties one would expect h and k values within the range $h = [0.36,0.44]$ and $k = [2.9,3.1]$, respectively.

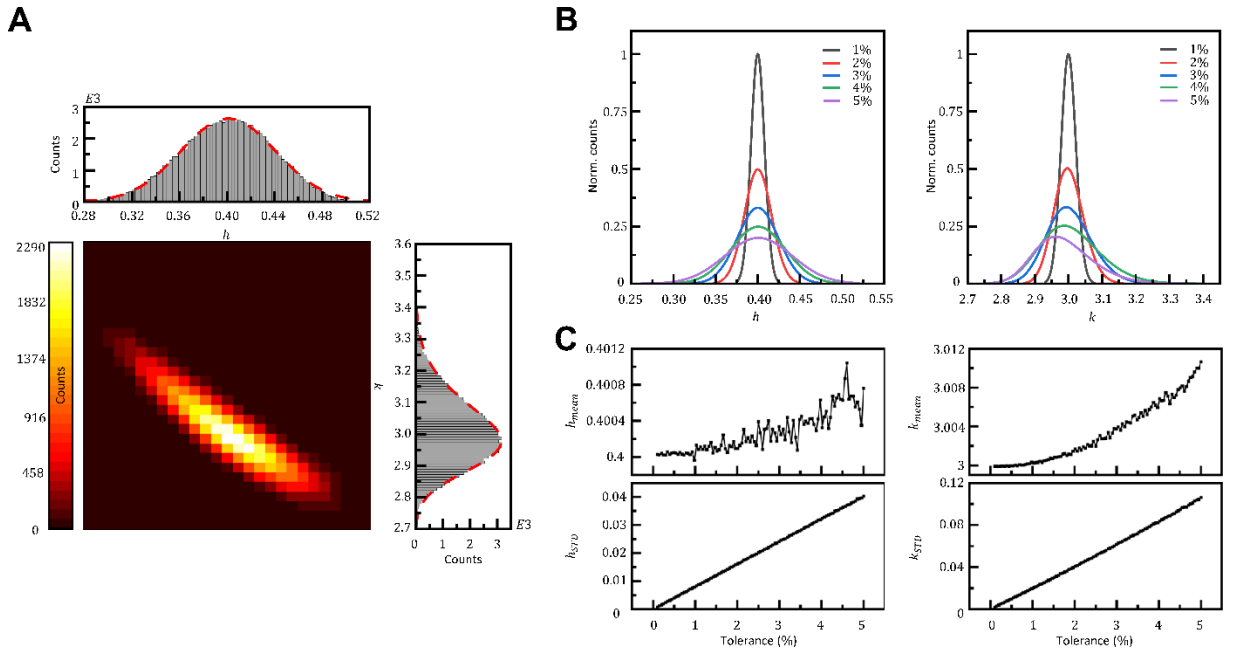

Fig. S8. Distribution of h and k values using tolerances on T-circuit parameters and properties. (a) 2D histogram showing the distribution of h and k values around $h = 0.4003$ and $k = 2.999$ when the T-circuit parameters and properties (L_1, L_2, L_3, L_4, w_{s1}, w_{s2}, w_p, ε_{s1}, ε_{s2}, ε_p) are allowed to vary by 5% around their desired values ($L_1 = L_4 = 7.394$ mm, $L_2 = L_3 = 7.307$ mm, $w_{s1} = w_{s2} = 0.2111$ mm, $w_p = 0.1911$ mm, $\varepsilon_{s1} = \varepsilon_{s2} = 21.5$ and $\varepsilon_p = 12$). (b) Normalized fitted distribution of h (left) and k (right) for tolerances from 1% to 5%. (c) Calculated mean (top-panels) and standard deviation (bottom-panels) of the fitted h (left) and k (right) distributions for tolerances from 1% to 5%.

6 Time domain convergence of PDE solution

One important metric to describe the performance of the PDE solving structure is the convergence time t_c. This is here defined as the time it takes for the PDE solving structure to reach a steady state solution. This can be quantified by calculating the rate of change in the signal observed at the waveguide junctions as:

$$convergence = \frac{d}{dt}\left(\sum_{junctions} |H_y| \right) \tag{S18}$$

where H_y is the out-of-plane H-field calculated at the junction centers and the sum covers all junctions within the waveguide network. t_c is then the time it takes for $convergence$ to approach 0 (while ignoring the trivial $H_y = 0$ case), within a certain tolerance value.

To investigate this, a time-domain numerical study of the structure presented in Fig. 2d of the main text was performed using the transient solver from CST Studio Suite®. Here, at time $t = 0$ a monochromatic 10 GHz input signal is excited at the top-left waveguide of the top-left junction. The out-of-plane H_y field is then recorded at the center of each of the 625 junctions and used to calculate the convergence value. The simulation is run for 50 ns from the initial excitation to allow it to reach steady state. As examples, the normalized $|H_y|$ values measured at 3 points P_1, P_2 and P_3 are shown in Fig. S9b. The location of these probe in the PDE solving structure can be seen in Fig. S9a. P_1 is the top-left boundary junction, P_2 is 15 junctions along and down from P_1 and P_3 is the bottom-right boundary junction (junction farthest from the input junction). Fig. S9c shows the $convergence$ value calculated from Eq. S18 and then normalized with respect to the maximum value.

It is expected that the convergence time of the PDE solving structure will depend primarily on the size of the network as the EM signals will take more time to propagate

throughout. This can be seen in Fig. S9b where P_2 and P_3 show initially zero out-of-plane H-field before the signal from P_1 arrives at the junction. This initial propagation time can also be seen in Fig. S9c where the initial rapid growth in $convergence$ value is indicative of the input signal spreading throughout the network. The maximum $convergence$ value then occurs at $\approx 5\,ns$, which is the theoretical time it takes for a signal to propagate from the top-left to the bottom-right junction when accounting for the lack of diagonal paths. After this, the $convergence$ value of the structure begins to decrease as the structure settles into the solution shown in Fig. 2d in the main text until after $t_c \approx 30$ ns there is little change in the PDE profile. It is worth noting that this calculated value of t_c is specific to the waveguide network from Fig. 2d waveguide network (25×25, designed to work at 10 GHz) and would need to be recalculated if the size, shape or operating frequency is changed. However, it is expected that changing the impedance values of the metatronic elements would not have a significant impact on t_c as the dielectric slabs used to implement the impedances are thin (in the direction of propagation) compared to the waveguide in which they are embedded.

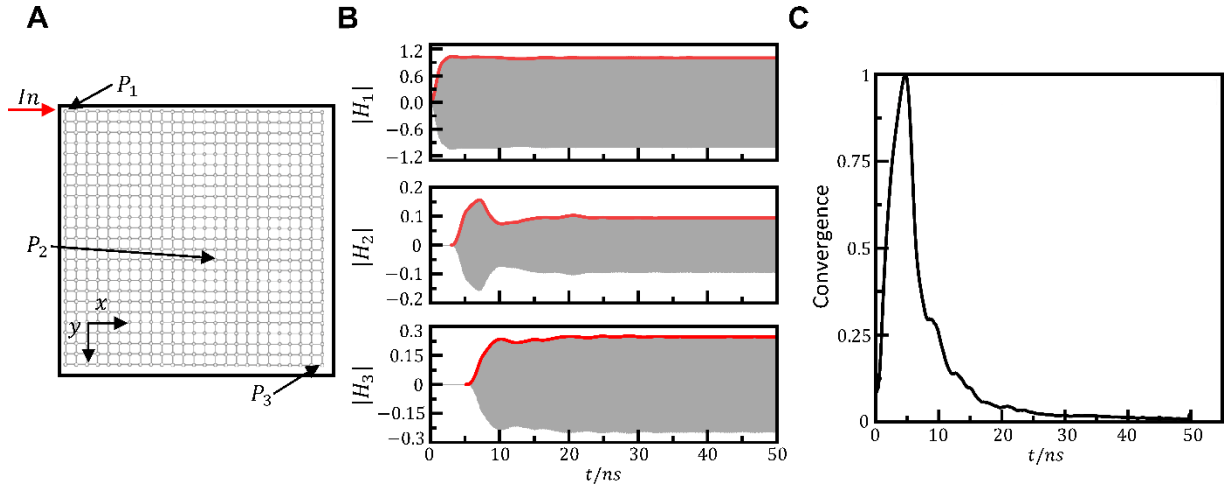

Fig. S9. Time domain convergence of structure from Fig. 2d. (a) Location of the three probes P_1, P_2 and P_3. (b) Calculated out-of-plane H_y-field at P_1, P_2 and P_3 as a function of time. (c) Normalized convergence plot of the total H_y-field present in the structure

7 Index of supplementary movies

- Supplementary Movie 1: Animation of Fig. 2d from the main text.
- Supplementary Movie 2: Animation of Fig. 2e from the main text.
- Supplementary Movie 3: Animation of Fig. 3b from the main text.
- Supplementary Movie 4: Animation of Fig. 3d from the main text.